Fatigue fractures and microstructure in Al-Cu-Mg machinable wrought alloys

J. Faltus[1]*, J. Siegl[2]

[1] *Research Insitute for Metals, Panenské Břežany, Ltd., Panenské Břežany 50, 250 70 Odolena Voda, Czech Republic*
[2] *Czech Technical University in Prague – Faculty of Nuclear Science and Physical Engineering, Trojanova 13, 120 00 Prague 1, Czech Republic*

Received 12 September 2006, received in revised form 8 November 2006, accepted 13 November 2006

Abstract

The article deals with microstructure and fatigue properties of machinable AA2007-T2 and AA2015-T2 aluminium alloys. The extruded and drawn rods of diameter of 19 mm were used for fatigue tests. Rods were manufactured in the plant of Alcan Děčín, Ltd. by a usual production method. The process of fatigue crack initiation and growth was qualitatively identical for both alloys. The fatigue crack initiation took place on the surface of test body notches, followed by crystallographic and striation phases of fatigue crack growth with the final ductile fracture. Fatigue lifetimes of the AA2015-T2 alloy compared to the AA2007-T2 alloy were higher in the whole tested area of cyclic stresses. This was caused by higher share of hard brittle particles containing Fe in the AA2007-T2 alloy, which resulted in an easier initialization of fatigue cracks and accelerated propagation. The higher content of low-melting metals and higher area share of soft particles of low-melting metals in the AA2015-T2 alloy, compared to the AA2007-T2 alloy, did not adversely affect the alloy fatigue performance.

K e y w o r d s: machinable aluminium alloys, microstructure, fatigue test, fractographic analysis, mechanisms of fatigue crack growth

1. Introduction

The alloying low-melting metals, lead and bismuth (from 0.5 to 1.5 wt.%) are used to increase machinability of 'free-cutting' aluminium alloys. However, the current European Communities regulations significantly limit the toxic lead content of metals. For instance, the maximum permissible lead content in wrought aluminium alloys used in means of transport is 0.4 %. In co-operation of two companies, VÚK Panenské Břežany, Ltd. and Alcan Děčín, Ltd., three types of new free-cutting aluminium alloys replacing lead with tin were developed [1–4]. Now, free-cutting aluminium alloys are often used in the automotive industry with increasing requirements not only for their mechanical properties but also for their fatigue and corrosion behaviour. At present, only partial knowledge of the influence of lead and bismuth contents on the fatigue performance of machinable (free-cutting) aluminium alloys is available, while data about the influence of tin on the fatigue behaviour of aluminium alloys is completely missing. Admittedly, the basic research on machinable aluminium alloys is complete, but knowledge of the fatigue performance is still not available for all types of alloy. The objectives of our work stemmed from this situation, i.e., to establish the fatigue performance of the new machinable aluminium alloys compared to the traditional lead-containing ones. The presented results, gained by measuring the fatigue performance of series 2xxx machinable alloys, are directly tied to the study of fatigue performance of series 6xxx aluminium machinable alloys [5, 6].

2. Materials and experimental procedures

2.1. M a t e r i a l s

Fatigue tests were performed on 19 mm diameter extruded and drawn rods made of Al CuMgMnSn-

*Corresponding author: tel.: +420 2 8397 0659; fax: +420 2 8397 0587; e-mail address: jiri.faltus@cbox.cz

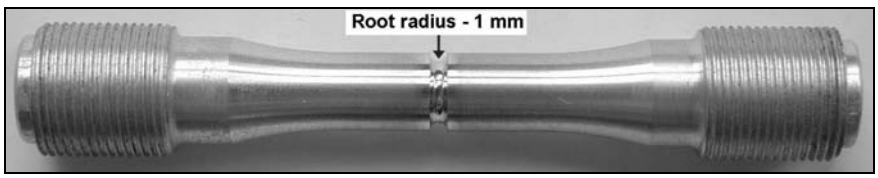

Fig. 1. Fatigue specimen, U-groove, root radius – 1 mm.

Bi (AA2015) lead-free machinable alloy and lead--containing Al Cu4PbMgMn (AA2007) alloy. The rods were prepared under normal manufacturing conditions in Alcan Děčín – Extrusions, Ltd. Both alloy rods were in the temper after the hot extruding with consequent quenching in the water wave behind the press, calibration drawing with 1.7 % reduction and natural ageing to the T2 temper. Table 1 shows the chemical composition of the tested alloys.

2.2. Experimental procedures

The metallographic analyses of the tested alloy rods were performed by the light microscopy method using a NIKON EPIPHOT 200 with a HITACHI three-chip colour camera for the image analysis and LUCIA software supplied by Laboratory Imaging, and the scanning electron microscopy method (SEM) plus local electron microprobe (EM) analysis using a DSM 940 microscope with a MICROSPEC WDX--3PC wave spectrometer. The analyses were conducted on lengthwise centreline sections. The grain boundaries were evaluated after electrolytic etching using Barker's method. The SEM method was used for the alloying element layouts for phase identifications.

Mechanical properties were determined using the universal testing machine Instron 55R1185 (100 kN) by a standard method of tensile test using circular specimens with a diameter of 7 mm, taken in the longitudinal axis of final rods.

Fatigue tests. For the fatigue tests, 9.3 mm in diameter cylindrical fatigue specimens with a notch of $K_t = 2.0$ (K_t – elastic stress concentration factor) and with M16×1 die heads were used (Fig. 1) [7]. Specimens were tested with 85 to 100 Hz frequencies and stress ratio $R = S_{min}/S_{max} = 0$ at 25 °C. Here S_{min} – minimum stress, S_{max} – maximum stress. The RUMUL Testronic 8601 100 kN high-frequency pulsator was used for the tests. They were performed with both alloys at six stress levels: at $S_{max} = 250, 230, 210, 190, 170$ and 150 MPa; two to six fatigue specimens were tested at these levels. The fatigue test results were evaluated using Wöhler curves.

Fractographic analysis. Morphology evaluations of separate fractures were performed under the light stereomicroscope at magnification of 4 to 75. A JSM 840A scanning electronic microscope with digitized image recording was used to analyse microfractographic marks. In the detailed fractographic analysis, special attention was paid both to the initiation regions of fatigue cracks and monitoring the micromorphologic characteristics of their development.

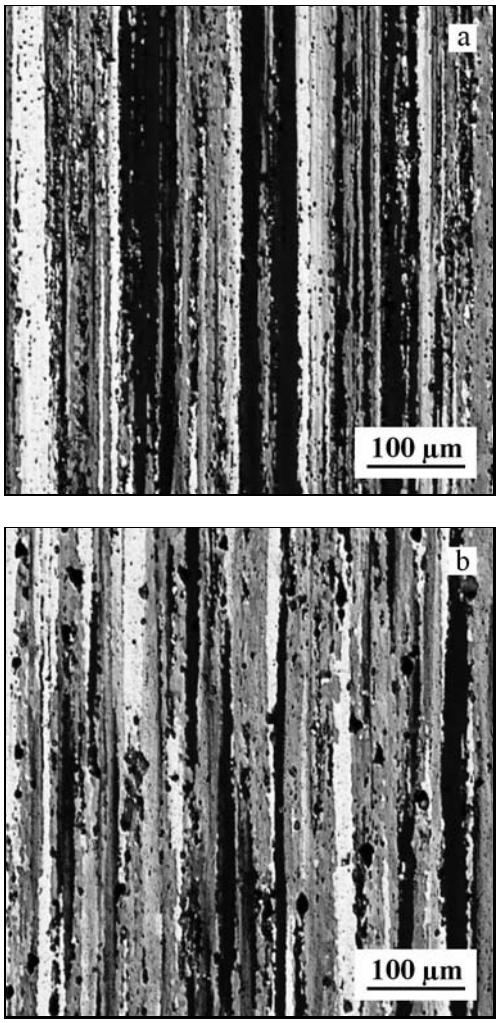

Fig. 2. Unrecrystallized "fibrous" structure of rods of AA2015-T2 alloy (a) and AA2007-T2 alloy (b).

3. Results and discussion

3.1. Microstructure

From the light microscopy point of view, the rod structure in the T2 state of both tested alloys AA2015 and AA2007 was fibrous, without any recrystallized surface zones (Fig. 2).

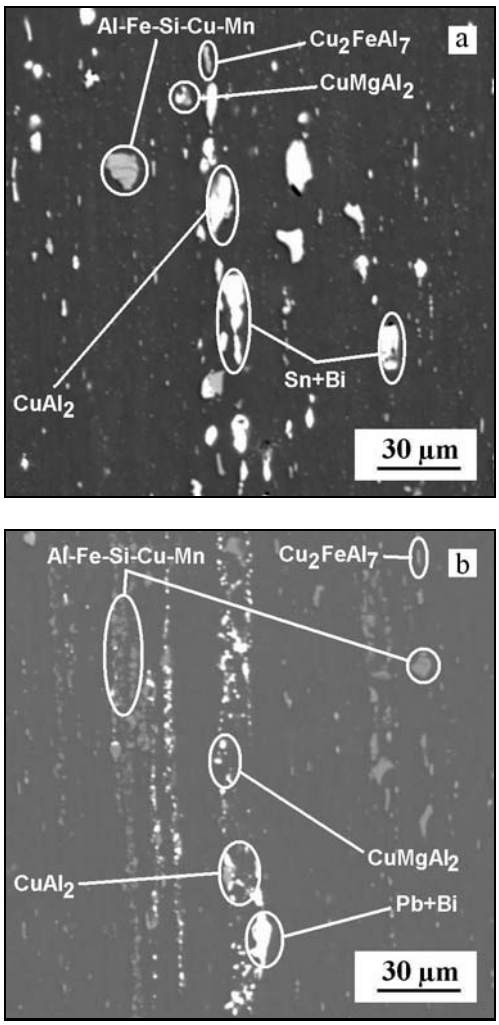

Fig. 3. SEM image of the structure of AA2015-T2 (a) and AA2007-T2 (b) in BSE mode – longitudinal section.

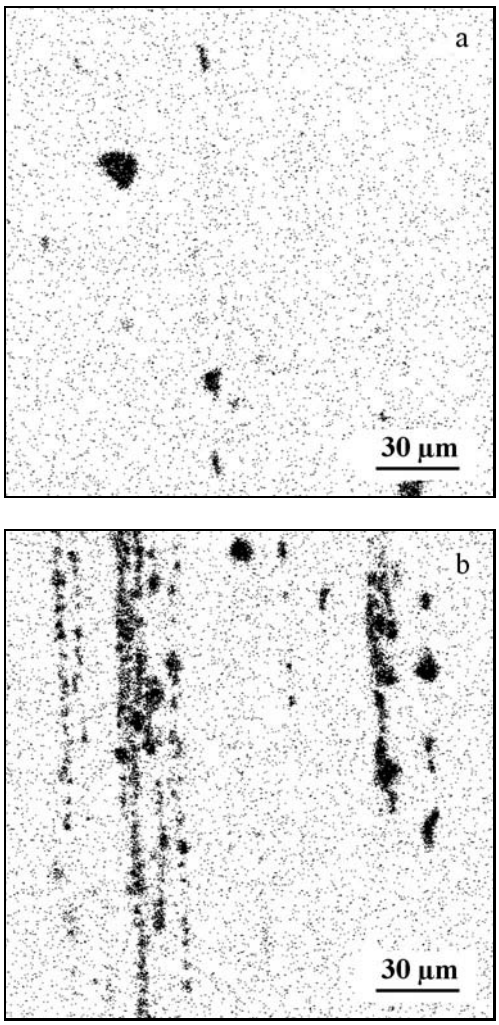

Fig. 4. Distribution of particles containing iron in AA2015-T2 alloy (a) and AA2007-T2 alloy (b), longitudinal section.

The analyses using SEM showed that both alloy microstructures contained particles of complex secondary intermetallic compound phases Al-Fe-Si-(Cu-Mn) with changing contents of alloying elements, phases containing aluminium, copper and iron (Cu_2FeAl_7), and undissolved phases $CuMgAl_2$ and $CuAl_2$ [8]. Furthermore, both alloys contained phase dispersion particles with a content of low-melting metals – either Sn or Bi (AA2015), or Pb and Bi (AA2007) (see Fig. 3). In both alloys, the phases were arranged in lines running in the pressing direction and they were slightly finer on the rod surface areas than those located in the mid-regions. A significant difference was noted between the structure of both alloys in the case of quantities and densities of the Fe-containing hard phases. Pressed and drawn parts made of AA2007 alloy had coarser Al-Fe-Si-(Cu-Mn) and their density was significantly higher compared to the AA2015 alloy (see Fig. 4). These different structures were caused by the fact that the iron content – as the decisive component in these phases – was almost tripled in the

Table 1. Chemical composition (in wt.%)

Alloy	Si	Fe	Cu	Mn	Mg	Cr	Zn	Ti	Pb	Bi	Sn	Others	Al
AA2015	0.710	0.210	4.240	0.593	0.888	–	0.010	0.030	0.030	0.311	1.040	0.15	Bal
AA2007	0.730	0.560	4.151	0.684	0.852	0.073	0.190	0.027	0.900	0.114	–	0.15	Bal

Table 2. The tensile test results of AA2015-T2 and AA2007-T2 measured on smooth specimens and fatigue specimens with a notch $K_t = 2.0$

Alloy	Smooth specimen	Specimen with a notch $K_t = 2.0$
AA2015-T2	$R_m = 503$ MPa, $R_p0.2 = 387.5$ MPa, $A5 = 11.4$ %	$R_m^K = 567$ MPa, $R_p0.2^K = 511$ MPa
AA2007-T2	$R_m = 442$ MPa, $R_p0.2 = 328$ MPa, $A5 = 13$ %	$R_m^K = 518$ MPa, $R_p0.2^K = 459$ MPa

AA2007 alloy compared to the AA2015 alloy (see Table 1).

The AA2015-T2 alloy contained phase dispersion particles with tin and bismuth, while the AA2007-T2 alloy dispersion particles contained lead and bismuth. The aggregate Sn & Bi content in the AA2015 alloy was 1.31 wt.%, while the Pb & Bi content was only 1.01 wt.%. Taking into account the lower density of tin than that of lead, it is not surprising that the number of surface share sections containing low-melting elements in the AA2015 alloy structure, which is 0.45 %, substantially outweighs the surface share of these phases in the AA2007-T2 alloy structure, which accounts for only 0.25 %. The layout of phases of low-melting metals in the structure of rods made of AA2015-T2 was more uniform than rods made of AA2007-T2 (see Fig. 3).

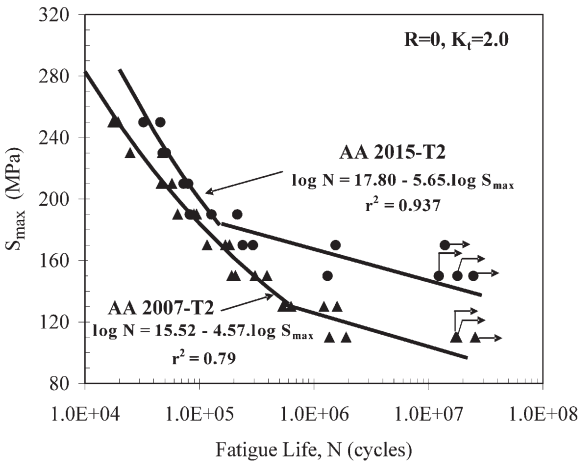

Fig. 5. *S-N* fatigue curves for AA2015-T2 and AA2007-T2 (N – cycles to failure).

3.2. Mechanical properties

The tensile test results of the alloys in the T2 temper measured on smooth specimens 7 mm in dia. (R_m, $R_p0.2$, $A5$) and on fatigue specimens with a notch of $K_t = 2.0$ (R_m^K, $R_p0.2^K$) are shown in Table 2. The results revealed the following facts: AA2015 alloy rods in the T2 temper containing tin always had higher strength properties ($R_p0.2$ and R_m) compared to AA2007 lead-containing rods; the differences were approx. 60 MPa. Plastic properties, represented by $A5$ elongation, were slightly lower for the AA2015 alloy than for the AA2007 alloy (see Table 2). Similar differences in the strength properties in the T2 temper were seen also in tensile tests provided on fatigue specimens with a $K_t = 2.0$ notch. Because of the influence of notch effects, the strength properties ($R_p0.2^K$ and R_m^K) were higher than the values for smooth rods. The reason for different mechanical properties of both alloys was – firstly – the high Fe content in the AA2007 alloy compared to the AA2015 alloy. In this case, iron fixes copper to forming complex phases, such as Cu_2FeAl_7 and others, which in turn reduces the quantity of the precipitating phases of $CuMgAl_2$ and $CuAl_2$ and, thus, reduces the efficiency of the precipitation hardening [9].

3.3. Fatigue life

From the fatigue test results it is obvious that the *S-N* curve has a break for both alloys, shown by a steep increase in the spread of the results (see Fig. 5).

Therefore, the measured data could not be smoothed by a single function. The curves had to be divided into two parts. In the higher tensions area, the least-square method was used for the logarithmic formula of $N = a\,S_{max}^b$ (a, b are constants). The use of this function for data under the curve break (190 MPa for the AA2015 alloy and 130 MPa for the AA2007 alloy) resulted in deteriorated matching efficiency of the function, shown by the determination coefficient r^2. For the experimental data approximation in the area under the *S-N* curve break, a linear relationship in log N and S_{max} coordinates was used. Because of the large number of incomplete tests (the points marked with arrows), the course of the relevant part in the linear relationship is a rough estimate only. The graphically plotted results of fatigue tests clearly confirmed that the fatigue lifetime values of the AA2015-T2 alloy were, compared to the AA2007-T2 alloy, shifted in the whole tested region of tensile strength to higher values, which also applied to the breakpoint on the *S-N* curve.

3.4. Fatigue fracture

Because of the morphology initiation area, no significant differences were found between AA2015 &

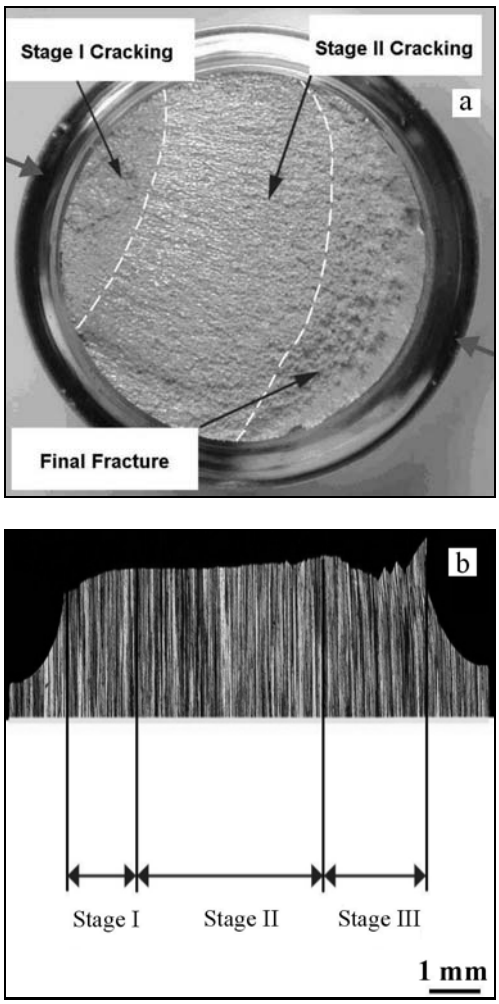

Fig. 6. Overall fracture surface of the sample 5-14-AA2015-T2 tested at 150 MPa, 1.3 mil. cycles to failure (a). Section through fracture area of the same sample 5-14-AA215-T2 (b).

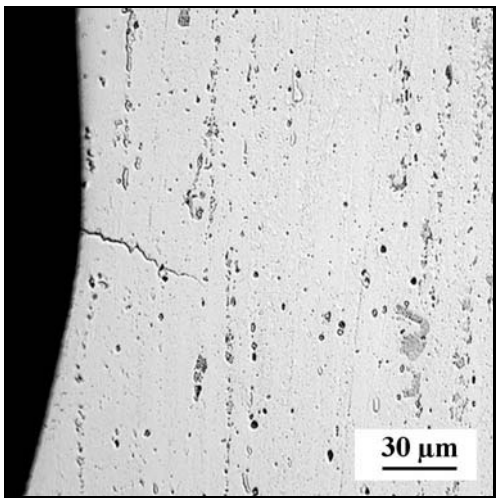

Fig. 7. Crack initiation at the bottom of the notch (AA2015-T2 sample, 250 MPa, 32 000 cycles).

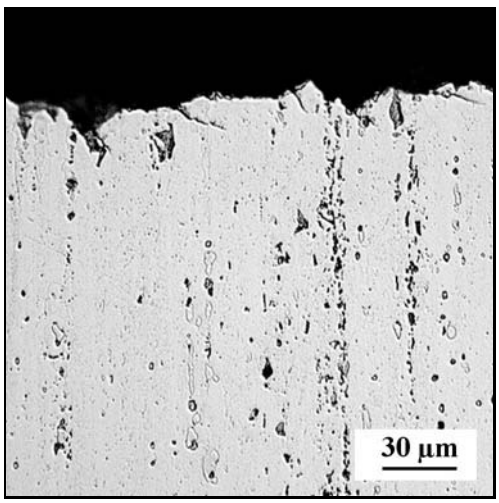

Fig. 8. Fatigue crack branching during stage I cracking (AA2015-T2 sample, 150 MPa, 1.3 million cycles).

AA2007 alloys. The process of fatigue failure was qualitatively identical for both alloys in the T2 temper, and according to the fracture morphology, it could be divided into three stages: (a) initiation and follow-up stage of crystallographic propagation of fatigue cracks, i.e., so-called "stage I cracking" [10], (b) propagation of fatigue cracks through the striations, i.e., so-called "state II cracking" [10] and (c) the final fracture of the rest of the load-bearing section through a ductile transcrystallic fracture (see Fig. 6).

Multiple crack initiations near the notch bottom and branching during the crystallographic propagation were noted with nearly all tested bodies (see Figs. 7 and 8). Since the structure was fibrous and non-recrystallized, the crack propagation in this stage of fatigue failure was mainly parallel to the maximum horizontal shear [10]. In Fig. 9, both alloys are compared according to their respective fracture surface micromorphologies in this propagation stage. The result of this comparison was that the fracture surface arrangement was finer with the AA2007-T2 alloy than with the AA2015-T2 alloy, which was supported by the higher density of hard iron-containing intermetallic phases.

After the initiation period and follow-up stage of crystallographic propagation of fatigue cracks, this failure became non-crystallographic. In principle, this fatigue crack propagation was perpendicular to the applied tension direction and followed the so-called striation mechanism. A comparison of the fracture surface arrangements in this fatigue crack propagation period for both alloys is shown in Fig. 10. Fundamental differences in the striation mechanism propagation morphology were not found for either material (AA2007-T2 & AA2015-T2).

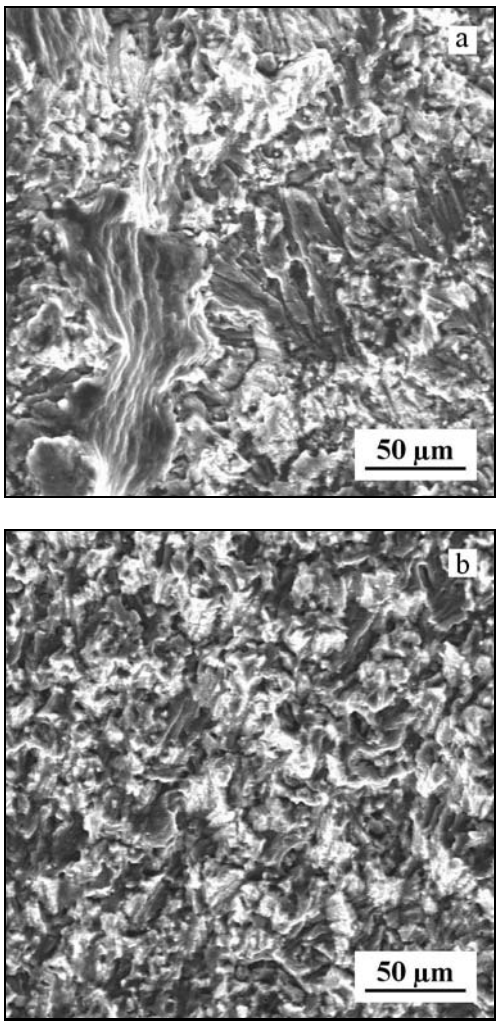

Fig. 9. Fracture micromorphology corresponding to crystallographic propagation of fatigue crack (stage I cracking) in AA2015-T2 sample (a) and AA2007-T2 sample (b).

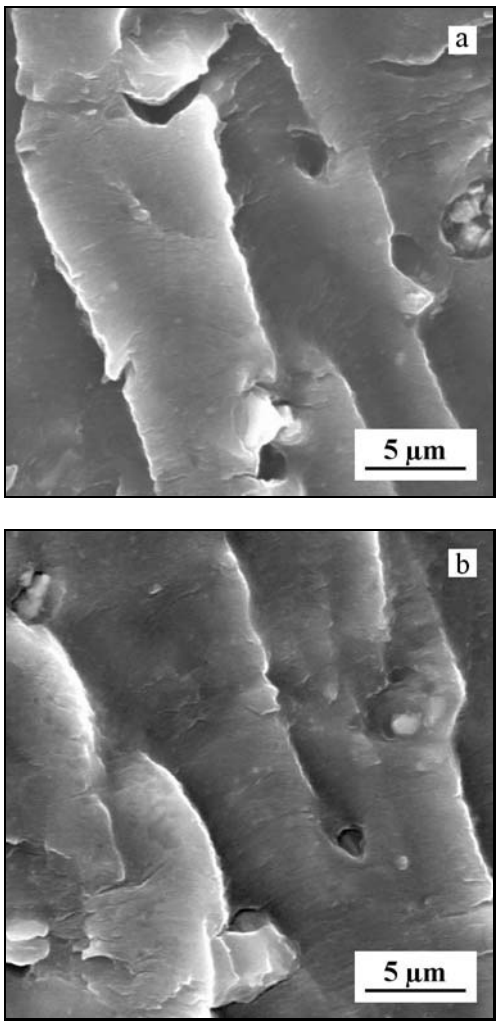

Fig. 10. Fracture micromorphology corresponding to striation mechanism propagation of fatigue crack (stage II cracking) in AA2015-T2 sample (a) and AA2007-T2 sample (b).

Finally, the third stage of the fatigue sample failure in the test was represented by a final rupture through a transcrystallic dimple fracture (see Fig. 11). From the fracture surface of both materials it was clear that the dimples created during the failure occurred mostly on the hard brittle particles of intermetallic phases, based on Al-Fe-Si-(Cu-Mn). They were either created by just a matrix decohesion from these hard phase particles, or preceded by a brittle failure of particles consequently initiating the matrix decohesion. Higher average sizes and density of phase particles containing iron in the structure of the AA2007-T2 alloy were accompanied by higher density of dimples with these phases on the bottom compared to AA2015-T2 (Fig. 11).

4. Conclusions

The fatigue tests analysis and study of microstructures of new machinable AA2015-T2 aluminium alloy (containing tin and bismuth) and commercial machinable AA2007-T2 aluminium alloy (containing lead) allowed us to do next conclusions:

(a) The secondary phase layouts in both alloy structures were qualitatively similar. The phases were arranged lengthwise in the pressing direction and they were slightly finer on the rod surface areas than those located in the mid-regions.

(b) The materials differed in their composition, layout and area share of low-melting metal particles; Sn + Bi particles in the AA2015-T2 alloy were more evenly distributed and their area share was higher compared to the Pb + Bi particles in the AA2007-T2 structure.

(c) A substantial difference between both alloys existed in the quantity and dimensions of hard and brittle intermetallic iron-containing phases Al-Fe-Si-(Cu-Mn). In the case of the AA2007-T2 alloy, these

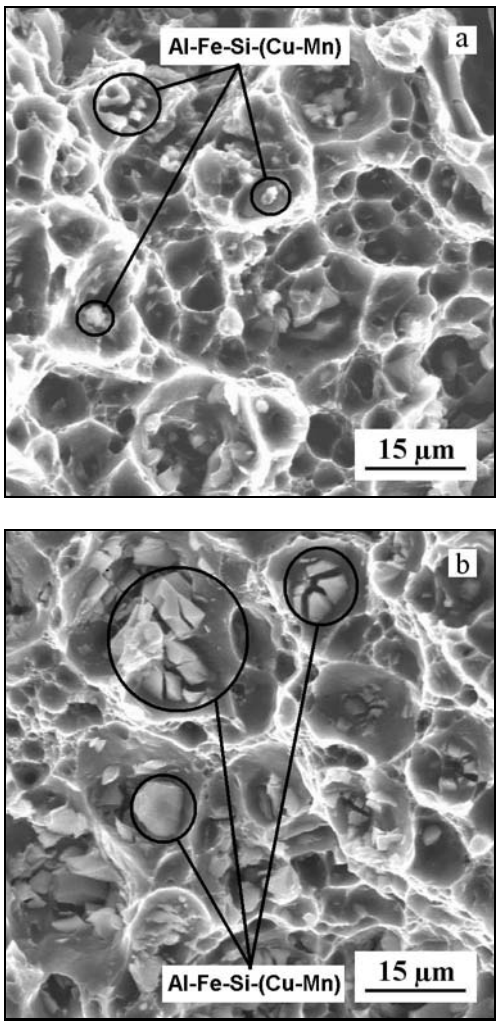

Fig. 11. Micromorphology of final fracture of AA2015-T2 sample (a) and AA2007-T2 sample (b).

phases were coarser and of higher density than in the AA2015-T2 alloy.

(d) Fatigue lifetimes of the AA2015-T2 alloy compared to the AA2007-T2 alloy were higher in the whole tested area of cyclic stresses. This was caused by the higher share of hard brittle particles with Fe content in the AA2007-T2 alloy, which resulted in an easier initialization of fatigue cracks and accelerated propagation.

Acknowledgements

This work was done as a part of the project Research Centre 1M2560471601 and project of Ministry of Education, Youth and Sports of the Czech Republic MSM 6840770021. The authors acknowledge also the company Alcan Děčín Extrusions, Ltd. for providing the experimental material. The authors acknowledge the contribution of Dr. V. Očenášek (VÚK Panenské Břežany, Ltd.) for providing and analysing of the fatigue tests.

References

[1] FALTUS, J.—PLAČEK, K.: Aluminium, *4*, 1999, p. 30.
[2] FALTUS, J.—PLAČEK, K.: Aluminium alloy with good machinability. Patent CZ 286 150, B6 (1996).
[3] FALTUS, J.—PLAČEK, K.: Aluminiumbegierung mit guter Spanbarkeit. European patent EP 9781069.4–1270, Prioritat: CZ 09.09.96, CZ 2628–96.
[4] FALTUS, J.—PLAČEK, K.: Bleifreie Aluminiumlegierung auf Basis von AlCuMg mit guter Spannbarkeit. Patent Nr. 98810537.5–2309, Anmeldetag: 12.6.98.
[5] FALTUS, J.—OČENÁŠEK, V.—SIEGL, J.—SLÁMA, P.: In: Proceedings 13. Internat. Metallurg. Symposium METAL 2004. Ed.: Prnka, T. Ostrava, vyd. Tanger, s.r.o. 2004, ISBN 80–5988–95–X (on CD-ROM).
[6] FALTUS, J.—SIEGL, J.—OČENÁŠEK, V.—ADÁMEK, J.: In: Proceedings 14. Internat. Metallurg. Symposium METAL 2005. Ed.: Prnka, T. Ostrava, vyd. Tanger, s.r.o. 2005, ISBN 80–86840–13–1 (on CD-ROM).
[7] FALTUS, J.—SIEGL, J.—OČENÁŠEK, V.—DALÍKOVÁ, K.: In: Proceedings 15. Internat. Metallurg. Symposium METAL 2006. Ed.: Prnka, T. Ostrava, vyd. Tanger, s.r.o. 2006, ISBN 80–86840–18–2 (on CD-ROM).
[8] MONDOLFO, L. F.: Aluminum Alloys: Structure and Properties of Nonferrous Alloys. London, Butterworth 1976.
[9] BROOKS, CH. R.: Heat Treatment, Structure and Properties of Nonferrous Alloys. Metals Park, Ohio, ASM 1984.
[10] STOLOFF, N. S.—DUQUETTE, D. J.: In: CRC Critical Reviews in Solid State Science. Boca Raton, FL, CRC Press 1974, p. 615.